Energy Materials

Supplementary Material

Flexible, highly conductive, and microscopically disordered MXene film electrode constructed via *in-situ* carbon dots intercalation toward high-performance supercapacitors

Deyu Yang[1,#], Haonan Cui[1,#], Razium Ali Soomro[1], Peng Zhang[1,2,*], Bin Xu[1,3,*]

[1]State Key Laboratory of Organic-Inorganic Composites, Beijing Key Laboratory of Electrochemical Process and Technology for Materials, Beijing University of Chemical Technology, Beijing 100029, China.
[2]Henan Key Laboratory of Quantum Materials and Quantum Energy, School of Quantum Information Future Technology, Henan University, Zhengzhou 450046, Henan, China.
[3]Shaanxi Key Laboratory of Chemical Reaction Engineering, School of Chemistry and Chemical Engineering, Yan'an University, Yan'an 716000, Shaanxi, China.
[#]Authors contributed equally.

Correspondence to: Dr. Peng Zhang, Henan Key Laboratory of Quantum Materials and Quantum Energy, School of Quantum Information Future Technology, Henan University, Mingli Street, Zhengzhou 450046, Henan, China. E-mail: pengzhang@henu.edu.cn; Prof. Bin Xu, State Key Laboratory of Organic-Inorganic Composites, Beijing Key Laboratory of Electrochemical Process and Technology for Materials, Beijing University of Chemical Technology, 15 Beisanhuan East Road, Chaoyang District, Beijing 100029, China; Shaanxi Key Laboratory of Chemical Reaction Engineering, School of Chemistry and Chemical Engineering, Yan'an University, 580 Shengdi Road, Yan'an 716000, Shaanxi, China. E-mail: xubin@yau.edu.cn/xubin@mail.buct.edu.cn

EXPERIMENTAL

Synthesis of $Ti_3C_2T_x$ MXene

A liquid phase etching method involving the LiF/HCl etchant was used for the synthesis of $Ti_3C_2T_x$ MXene. In a typical procedure, 0.99 g of LiF in 10 mL of HCl (12 M) was homogenized

to form an etchant solution. Next, 1 g of Ti_3AlC_2 was gradually added to the etchant under stirring at 35 °C for 24 h to etch the Al layers. The etched product was then washed with deionized water (DIW) multiple times, followed by centrifuging at 5200 rpm until the pH of the suspension was above 6. The precipitates were re-dispersed in DIW and ultrasonicated at 240 W for 30 min to exfoliate the multilayer $Ti_3C_2T_x$. Finally, the mixture underwent a centrifugation process at 5200 rpm for 1 h to separate single-layer $Ti_3C_2T_x$ MXene from its multilayer counterpart. The obtained dark $Ti_3C_2T_x$ dispersion was then sealed with Argon for future use.

Materials characterization

Microscopic techniques such as SEM (Hitachi S4800), transmission electron microscope (TEM, GEOL-JEM1400), and HRTEM (Tecnai G2 F30) were used for morphological assessment. SEM equipped with EDS confirmed the elemental composition, whereas XRD analysis (X'Pert-Pro MPD, PANalytical) with monochromatic Cu Kα radiation (λ=0.15418 nm, 5° min^{-1}) was used for compositional evaluation. Raman spectrometry was conducted using a Renishaw 1000 Raman spectrometer with 633 nm laser irradiation. XPS (ESCALAB 250Xi) was used for surface composition analysis, whereas WAXS and SAXS measurements were measured with XEUSS WAXS/SAXS system, equipped with a rotating anode X-ray source (operated at 30 W, λ=0.15418 nm) and a Pilatus 300 K detector. The WAXS and SAXS detectors were positioned 88 and 1185 mm from the samples. The electrical conductivity measurements were carried out using an RTS-8 four-probe tester. The water contact angle measurements were acquired using a JGW-360B contact angle tester.

Electrochemical measurements

The CDs-MF were cut into 5 mm diameter disks and directly employed as working electrodes for supercapacitors. A three-electrode system (Swagelok) configuration was adopted with activated carbon, Ag/AgCl, and 3 M H_2SO_4 solution as counter electrode, reference electrode, and electrolyte, respectively. CV and GCD measurements were conducted using a Chenhua electrochemical workstation (CHI 600E) and an Arbin BT2000 battery tester, respectively, over a potential range of -0.6~0.2 V (*vs.* Ag/AgCl). Bio-Logic electrochemical workstation (VSP) was used for electrochemical impedance spectroscopic measurements in a frequency range from 100 kHz to 10 mHz. The flexible quasi-solid-state symmetric supercapacitor was assembled applying the CDs-MF-2, 3 M H_2SO_4/PAA gel, and nonwoven fabric (NKK-MPF30AC) as the working electrode, electrolyte, and separator, respectively.

Electrochemical calculations

In three-electrode system, the gravimetric specific capacitances (C_g) based on the GCD and CV curves were calculated according to the following **Supplementary Equation (1)** and **(2)**, respectively:

$$C_g = \frac{It}{\Delta V m} \tag{1}$$

$$C_g = \frac{1}{\Delta V m v} \int i dv \tag{2}$$

where *I* is the current (A), t is the discharge time (s), ΔV is the potential window (V), and m is the mass of working electrode (g).

The *b* values of the electrodes were obtained through the relationship of current (*i*) and scan rates (*v*) according to the following power law:

$$i = av^b \tag{3}$$

where the *b* functions as an indicator that reflect the charge storage kinetics. A *b* value of 0.5 indicates the entirely diffusion-controlled contribution, while *b*=1 signifies the complete capacitive-dominated contribution in the total capacitance.

The specific capacitive contributions at different scan rates could be determined through the **Supplementary Equation (4)**:

$$i(v) = k_1 v + k_2 v^{1/2} \tag{4}$$

where the $k_1 v$ and $k_2 v^{1/2}$ are the capacitive-dominated and diffusion-controlled currents, respectively.

The real C′(ω) and imaginary part C″(ω) capacitances were calculated through the following **Supplementary Equations**:

$$C' = \frac{-Z''(f)}{2\pi f |Z(f)|^2} \tag{5}$$

$$C'' = \frac{Z'(f)}{2\pi f |Z(f)|^2} \tag{6}$$

$$\tau_o = {}^{1}/_{f_0} \tag{7}$$

where $Z'(f)$ and $Z''(f)$ are the real and imaginary parts of the $Z(f)$, respectively, τ_0 is the relaxation time constant, f stands for the frequency, and f_0 represents the frequency at the maximum C".

In flexible SSC device, the capacitance was calculated based on the total mass of both anodic and cathodic electrodes according to the **Supplementary Equation (2)**. The gravimetric energy

density (E_g), gravimetric power density (P_g), and volumetric energy density (E_v) were calculated through the following **Supplementary Equations**, respectively:

$$E_g = \int VIdv/m \tag{8}$$

$$P_g = E_g/\Delta t \tag{9}$$

$$E_v = \rho E_g \tag{10}$$

where m and Δt are the total mass of the electrodes (kg) and discharge time (h), respectively.

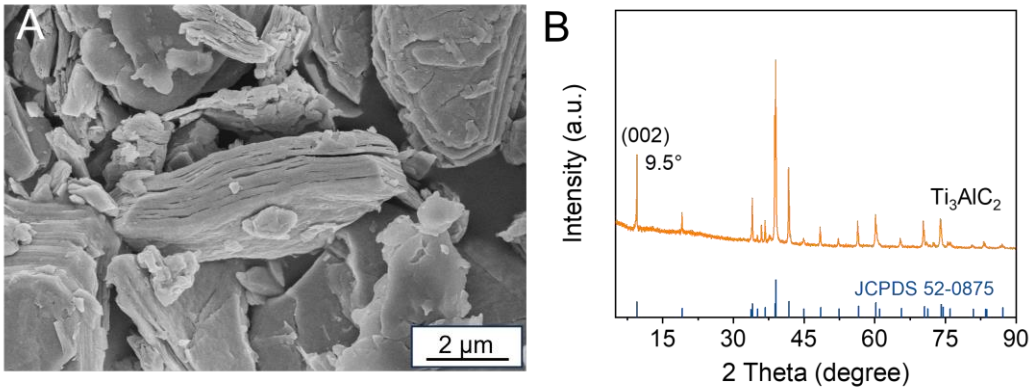

Figure S1. (A) SEM image and (B) XRD patterns of the Ti_3AlC_2 powders.

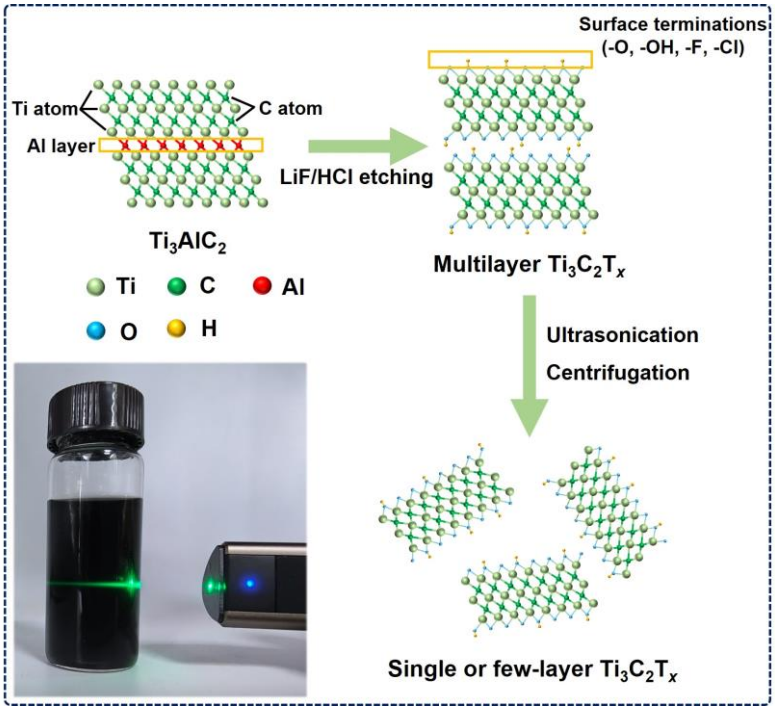

Figure S2. Schematic illustration for the fabrication process of $Ti_3C_2T_x$ MXene flakes, with inset digital image indicating the excellent dispersity in aqueous system.

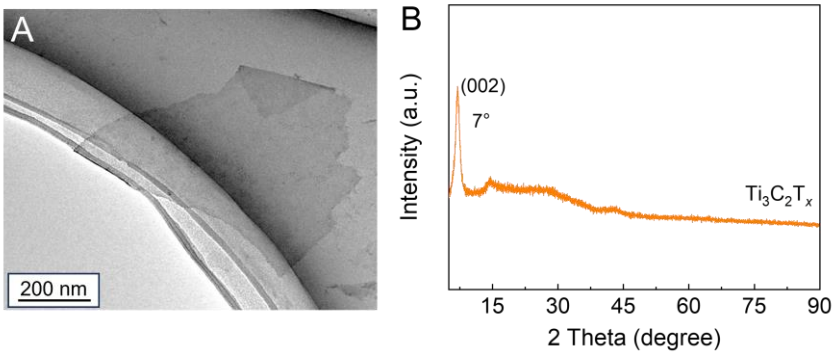

Figure S3. (A) TEM image and (B) XRD patterns of the $Ti_3C_2T_x$ MXene.

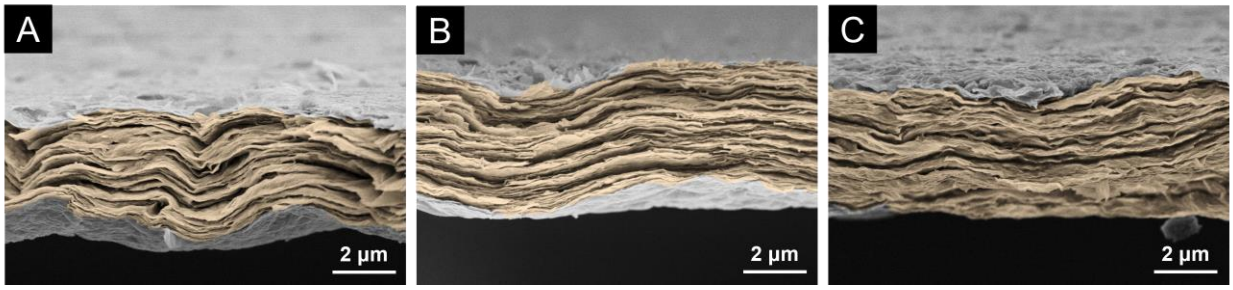

Figure S4. Cross-sectional SEM images of the (A) G-MF-1, (B) G-MF-2, and (C) G-MF-3.

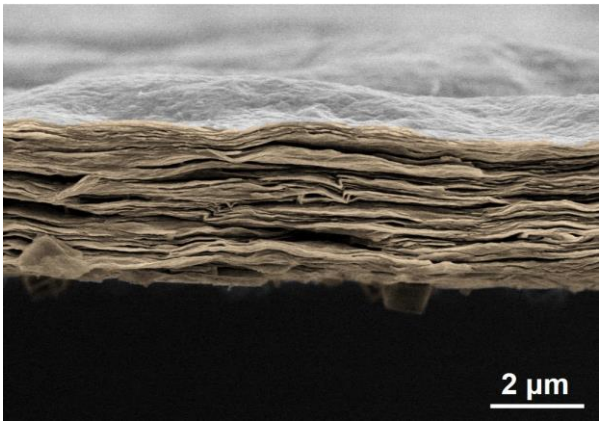

Figure S5. Cross-sectional SEM image of the a-MF.

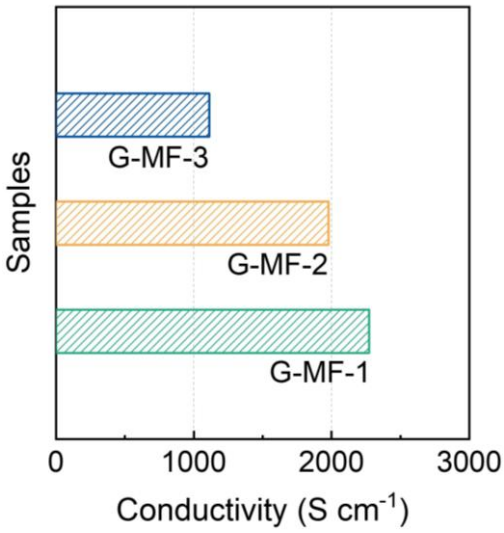

Figure S6. Electrical conductivities of the MXene/gelatin films.

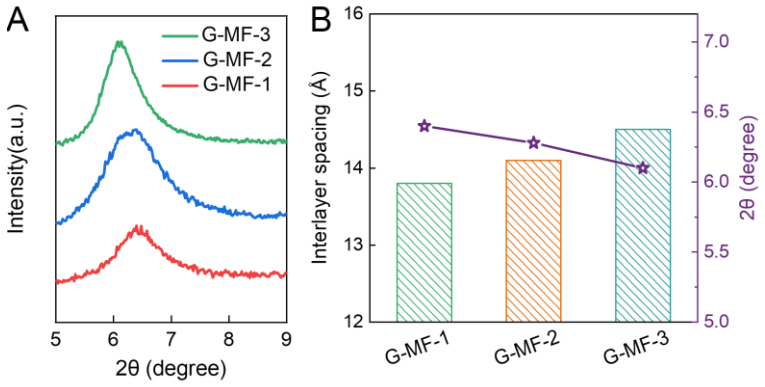

Figure S7. (A) XRD patterns of the G-MF with (B) corresponding summary depicting their (002) peak locations and interlayer spacings.

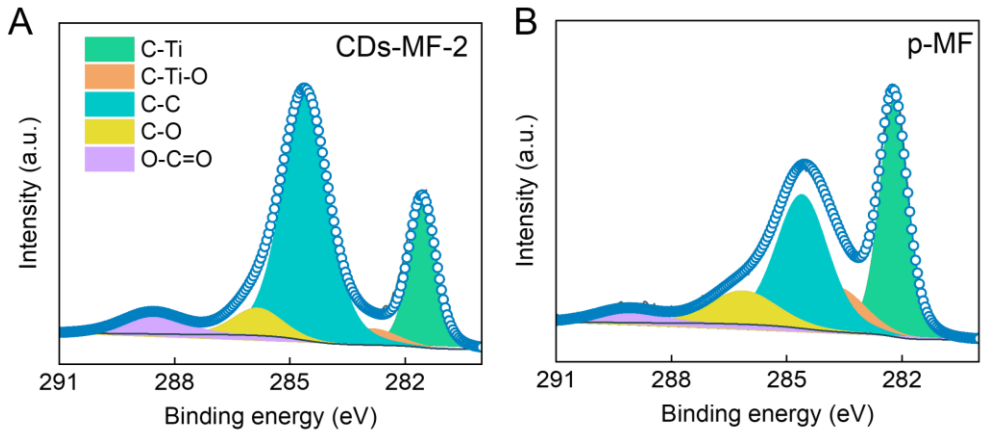

Figure S8. High-resolution C 1s spectra of the (A) CDs-MF-2 and (B) p-MF.

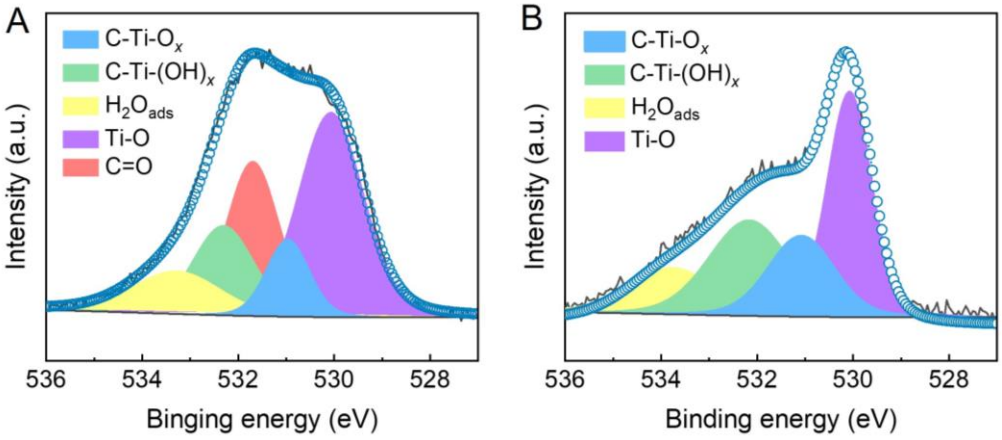

Figure S9. High-resolution O 1s spectra of the (A) CDs-MF-2 and (B) p-MF.

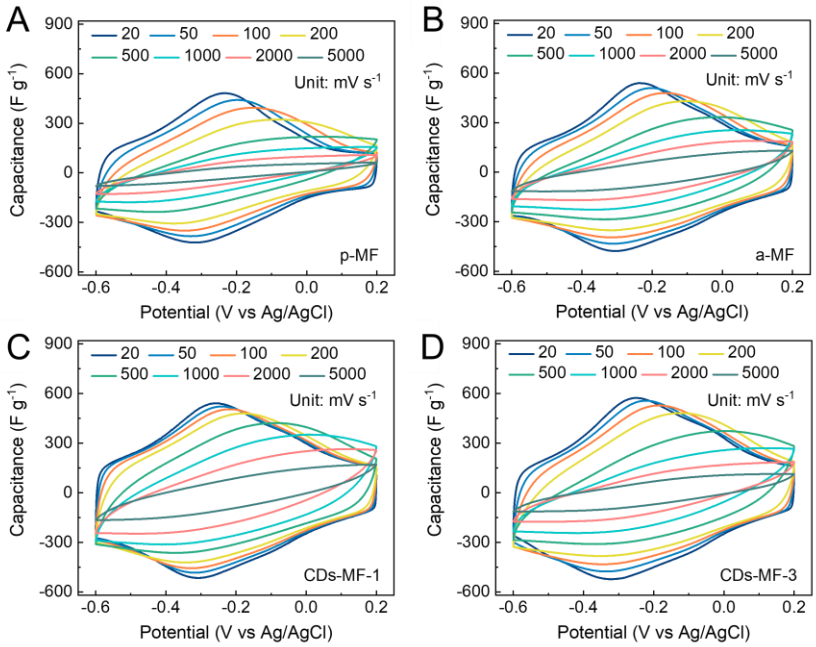

Figure S10. CV curves of the (A) p-MF, (B) a-MF, (C) CDs-MF-1, and (D) CDs-MF-3 at various scan rates from 20 to 5000 mV s^{-1}.

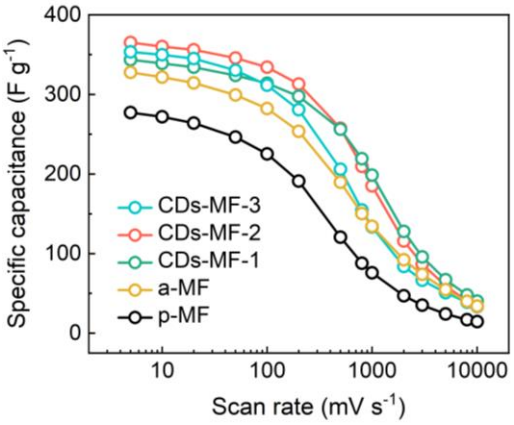

Figure S11. Gravimetric capacitances of the CDs-MF, a-MF, and p-MF at different scan rates.

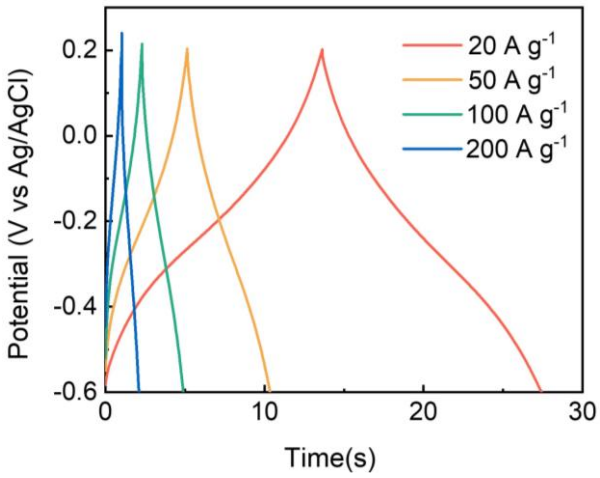

Figure S12. GCD curves of the CDs-MF-2 at different current densities of 20, 50, 100, and 200 A g^{-1}.

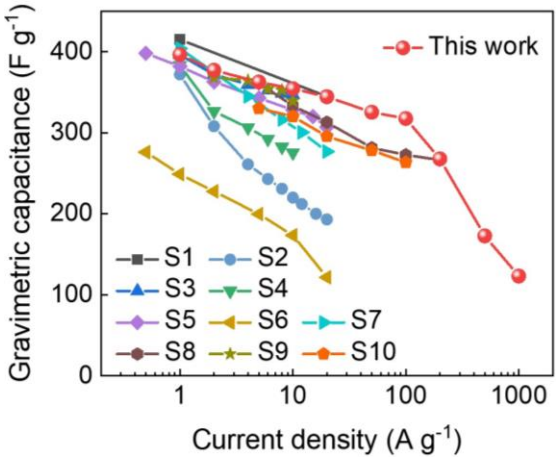

Figure S13. Comparison of the rate performance of CDs-MF-2 with other previous reports.

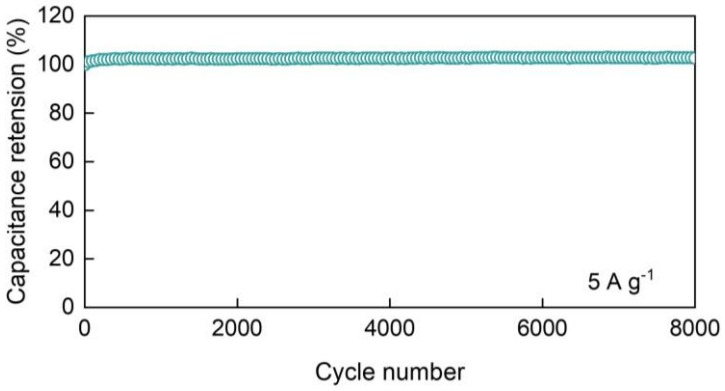

Figure S14. Long-term cycle performance of the CDs-MF-2 at 5 A g^{-1}.

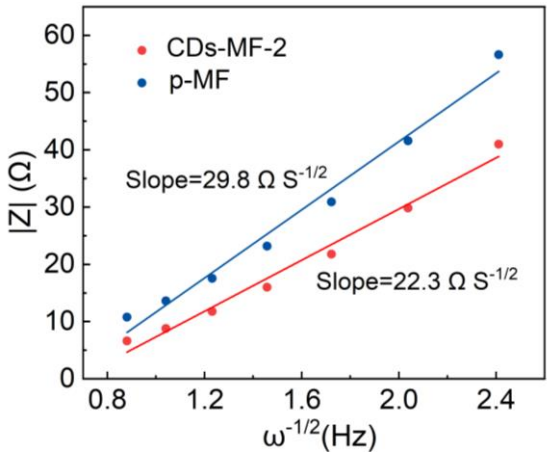

Figure S15. Linear fit showing the relationship between Z' and $\omega^{-1/2}$ of the CDs-MF-2 and p-MF in the low-frequency region.

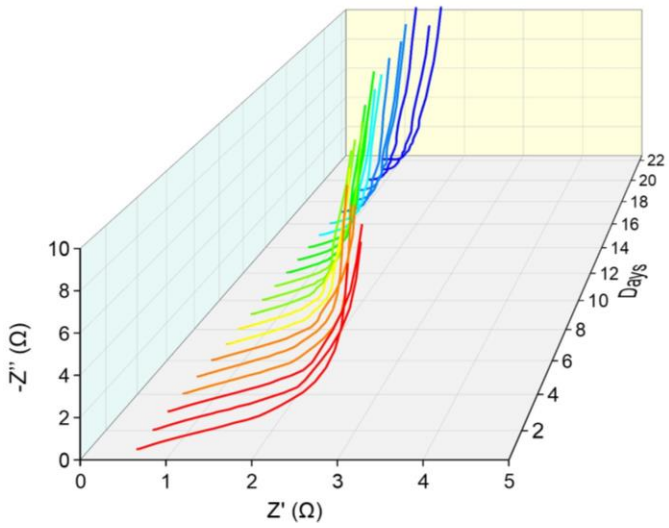

Figure S16. Daily EIS plots of the CDs-MF-2 electrode during a 21-day immersion in 3 M H_2SO_4 electrolyte.

Table S1. Summary of the gravimetric and volumetric capacitances of the CDs-MF, a-MF, and p-MF at various current densities and scan rates.

	Gravimetric capacitances								**Volumetric capacitances**			
	Current density (A g^{-1})				**Scan rate (mV s^{-1})**				**Current density (A cm^{-3})**			
	1	**10**	**100**	**1000**	**5**	**100**	**1000**	**5000**	**1**	**10**	**100**	**1000**
CDs-MF-1	381.5	335.8	297.6	85.4	343.5	314.0	198.6	67.1	1347.0	1278.2	1212.1	826.8
CDs-MF-2	396.4	354.4	317.5	123.2	365.2	334.3	185.1	59.4	1153.2	1073.7	1004.9	611.3
CDs-MF-3	360.3	320.1	272.2	36.7	353.3	311.5	133.4	50.9	1032.0	947.7	805.1	287.5
a-MF	325.7	285.3	205.8	36.6	327.7	282.1	134.2	54.8	1290.8	1175.4	1032.7	399.7
p-MF	258.8	228.8	132.2	11.9	277.2	225.1	75.8	24.1	847.6	780.3	652.4	274.8

Reference

[S1] Zhu Z, Wang Z, Ba Z et al. 3D MXene-holey graphene hydrogel for supercapacitor with superior energy storage. *J Energy Storage* 2022;47:103911. [DOI: https://doi.org/10.1016/j.est.2021.103911]

[S2] Zhang X, Liu Y, Dong S, Yang J, Liu X. Flexible electrode based on multi-scaled MXene ($Ti_3C_2T_x$) for supercapacitors. *J Alloy Compd* 2019;790:517-523. [DOI: https://doi.org/10.1016/j.jallcom.2019.03.219]

[S3] Wu Q, Xue Y, Li P, Wang Y, Wu F. High specific capacitance and long cycle stability of few-layered hexagonal Ti_3C_2 free-standing film constructed with spiral chiral Hexagon Ti_3AlC_2. Appl Surf Sci 2023;609:155329. [DOI: https://doi.org/10.1016/j.apsusc.2022.155329]

[S4] Guan G, Li P, Shi X et al. Electrode based on porous MXene nanosheets for high-performance supercapacitor. *J Alloy Compd* 2022;924:166647. [DOI: https://doi.org/10.1016/j.jallcom.2022.166647]

[S5] Gao G, Yang S, Wang S, Li L. Construction of 3D porous MXene supercapacitor electrode through a dual-step freezing strategy. *Scripta Mater* 2022;213:114605. [DOI: https://doi.org/10.1016/j.scriptamat.2022.114605]

[S6] Zhang J, Jiang D, Liao L, Cui L, Zheng R, Liu J. $Ti_3C_2T_x$ MXene based hybrid electrodes for wearable supercapacitors with varied deformation capabilities. *Chem Eng J* 2022;429:132232. [DOI: https://doi.org/10.1016/j.cej.2021.132232]

[S7] Zhang X, Liu X, Dong S, Yang J, Liu Y. Template-free synthesized 3D macroporous MXene with superior performance for supercapacitors. *Appl Mater Today* 2019;16:315-321. [DOI: https://doi.org/10.1016/j.apmt.2019.06.013]

[S8] Wei L, Deng W, Li S, Wu Z, Cai J, Luo J. Sandwich-like chitosan porous carbon Spheres/MXene composite with high specific capacitance and rate performance for supercapacitors. *J Bioresour Bioprod* 2022;7:63-72. [DOI: https://doi.org/10.1016/j.jobab.2021.10.001]

[S9] Liu L, Yin H, Guo W, Jia B, Jiang H. High gravimetric capacitance MXene supercapacitor electrode based on etched $Ti_3C_2T_x$ by chemical etching. *Adv Eng Mater* 2023;25:2201425. [DOI: https://doi.org/10.1002/adem.202201425]

[S10] Xu H, Fan J, Su H et al. Metal ion-induced porous MXene for all-solid-state flexible supercapacitors. *Nano Lett* 2023;23:283-290. [DOI: https://doi.org/10.1021/acs.nanolett.2c04320]